AGU PUBLICATIONS

JGR

Journal of Geophysical Research: Solid Earth

RESEARCH ARTICLE
10.1002/2014JB011504

Special Section:
Stress, Strain, and Mass Changes at Volcanoes

Stress changes, focal mechanisms, and earthquake scaling laws for the 2000 dike at Miyakejima (Japan)

Luigi Passarelli[1], Eleonora Rivalta[1,2], Simone Cesca[1,3], and Yosuke Aoki[2]

[1]GFZ German Research Centre for Geosciences, Potsdam, Germany, [2]Earthquake Research Institute, University of Tokyo, Tokyo, Japan, [3]Institute of Earth and Environmental Sciences, University of Potsdam, Potsdam, Germany

Key Points:
- FMs compatible with the calculated Coulomb stress changes induced by the dike
- Faulting styles induced by dike range from strike slip to oblique and normal faulting
- Normal faulting does not follow a Gutenberg-Richter statistics

Correspondence to:
L. Passarelli,
luigi@gfz-potsdam.de

Citation:
Passarelli, L., E. Rivalta, S. Cesca, and Y. Aoki (2015), Stress changes, focal mechanisms, and earthquake scaling laws for the 2000 dike at Miyakejima (Japan), *J. Geophys. Res. Solid Earth*, *120*, 4130–4145, doi:10.1002/2014JB011504.

Received 31 JUL 2014
Accepted 25 MAY 2015
Accepted article online 29 MAY 2015
Published online 24 Jun 2015

Abstract Faulting processes in volcanic areas result from a complex interaction of pressurized fluid-filled cracks and conduits with the host rock and local and regional tectonic setting. Often, volcanic seismicity is difficult to decipher in terms of the physical processes involved, and there is a need for models relating the mechanics of volcanic sources to observations. Here we use focal mechanism data of the energetic swarm induced by the 2000 dike intrusion at Miyakejima (Izu Archipelago, Japan), to study the relation between the 3-D dike-induced stresses and the characteristics of the seismicity. We perform a clustering analysis on the focal mechanism (FM) solutions and relate them to the dike stress field and to the scaling relationships of the earthquakes. We find that the strike and rake angles of the FMs are strongly correlated and cluster on bands in a strike-rake plot. We suggest that this is consistent with optimally oriented faults according to the expected pattern of Coulomb stress changes. We calculate the frequency-size distribution of the clustered sets finding that focal mechanisms with a large strike-slip component are consistent with the Gutenberg-Richter relation with a *b* value of about 1. Conversely, events with large normal faulting components deviate from the Gutenberg-Richter distribution with a marked roll-off on its right-hand tail, suggesting a lack of large-magnitude events ($M_w > 5.5$). This may result from the interplay of the limited thickness and lower rock strength of the layer of rock above the dike, where normal faulting is expected, and lower stress levels linked to the faulting style and low confining pressure.

1. Introduction

Propagating magma-filled dikes induce abundant seismicity containing a wealth of information on the dynamics of the magma and on its coupling with the host rock and the local tectonics. The earthquake hypocenters in dike-induced swarms are often observed to migrate [*Einarsson and Brandsdóttir*, 1980; *Aoki et al.*, 1999; *Keir et al.*, 2009; *Rivalta*, 2010; *Dahm et al.*, 2010; *Belachew et al.*, 2011; *Grandin et al.*, 2011; *Segall*, 2013; *Rivalta et al.*, 2014]. The pattern of migration has been linked to different factors, including stress concentrations migrating with the dike's tip [*Hill*, 1977; *Einarsson and Brandsdóttir*, 1980; *Rubin and Gillard*, 1998], the history of dike geometry and pressurization [*Roman*, 2005; *Uhira et al.*, 2005; *Traversa and Grasso*, 2009; *Dahm et al.*, 2010; *Rivalta*, 2010; *Traversa et al.*, 2010; *Traversa and Grasso*, 2010; *Segall*, 2013], the host rock rheology [*Rivalta and Dahm*, 2004], and the presence of active preexisting faults [*Rubin and Gillard*, 1998; *Rubin et al.*, 1998; *Toda et al.*, 2002; *Rivalta and Dahm*, 2004].

Given energetic seismic swarms and a good azimuthal coverage of seismic stations, focal mechanism (FM) solutions can be derived. Volcanic areas are often linked to a broad range of observed FMs, generally explained in terms of rock and stress heterogeneities. *Hill* [1977] discussed in a seminal paper the relation between focal mechanisms and surface structural trends reported for some swarm-like sequences, including the Reykjanes Peninsula in Iceland, Imperial Valley, and Hawaii. He derived a geometrical model involving oblique shear cracks joining the tips of pressurized opening fractures with different configurations of the most compressive, intermediate, and least compressive principal stresses, σ_1, σ_2, and σ_3, respectively. The model works both in plan view (explaining strike-slip FMs joining the opening cracks) and in cross section (explaining normal faulting FMs).

Brandsdóttir and Einarsson [1979] derived FM solutions for the September 1977 dike intrusion at Krafla (Iceland). They found that most FMs were predominantly normal faulting with variable strike-slip component. The nodal planes were steeply dipping, mostly striking parallel to the dike and consistent with most surface faults, which defined a graben with uplifted flanks. The focal mechanisms were, however, more variable than

one would expect from the observations of the surface faulting. In particular, the oblique components of the FMs remained unexplained.

Rubin and Pollard [1988] calculated the 2-D stress change due to an inflating dike in the presence of a vertical pressure gradient. The dike opening increases tension in the region above the tip, favoring normal faulting, and creates compression at the sides, inhibiting faulting. They also calculated the "slip tendency" by solving the Coulomb's law of friction $\|\tau\| \leq \mu\sigma_n$, with τ shear stress, μ friction, and σ_n normal stress.

Ukawa and Tsukahara [1996] studied the swarm-like seismicity recorded in the time frame 1982–1989 in the Izu Peninsula, Japan, including two large swarms in 1988 and 1989. Relocation of the earthquakes showed migration of the seismicity from large (~20 km) to shallow (~3 km) depths, consistent with dikes nucleating at and ascending from a deep dike-like reservoir. The *P* and *T* axes (pressure and tension axes, respectively) of the earthquakes were found to be mostly close to horizontal, indicating predominantly strike-slip earthquakes. The orientation of the *P* and *T* axes were deemed consistent with both the tectonic stress of the area and the orientation of the dike (*P* axes aligned with the dike and *T* axes perpendicular to it). The strike-slip earthquakes were interpreted loosely based on the model proposed by *Rubin and Pollard* [1988] as resulting from the regional stresses above the dike [*Ukawa and Tsukahara*, 1996, Figures 14b and 14c]. Such interpretation explains the main characteristics of the observation, but the oblique FMs remained unaddressed.

Shuler and Nettles [2012] investigated an intense seismicity swarm that occurred in November 2010 in the western Gulf of Aden. They derived moment tensor solutions for more than a hundred events with moment magnitude between 4.5 and 5.5. The predominantly shallow normal faulting events and an almost perfect alignment with the fault traces mapped for this ridge segment suggested that the swarm was triggered by a lateral dike intrusion. The along-rift migration of epicenters in the first few hours from the swarm onset also corroborated the hypothesis of seismicity induced by diking. Only a few strike-slip mechanisms being observed were interpreted as occurring onto a transform fault of the incipient rift-transform segmentation in the Gulf of Aden. All the events were very shallow, and the largest was estimated to have downdip fault dimension of about 5 km. The *b* value of the frequency-size distribution was estimated about 1.6.

Belachew et al. [2013] calculated the FMs of the earthquakes accompanying the November 2007 and October 2008 dikes in the Dabbahu-Manda Hararo rift segment in Afar, Ethiopia, with the purpose of clarifying how the seismic strain is partitioned between the rock volumes around the propagating dike tip and above the dike. The best double-couple mechanisms were mainly normal faulting with small strike-slip components, except for two earthquakes with dominant strike-slip component. Most earthquakes were shallow and occurred during the propagation phase of the dikes, while the two strike-slip events were particularly deep. The nodal planes struck parallel to the dike, consistent with the strikes of surface fault ruptures measured in the field and from satellite imagery. The conclusion of the study is that most of the seismic energy release during dike intrusions occurs by faulting above the dikes. Again, no interpretation is given for the oblique components in the FMs and for the two strike-slip events.

The examples above, which include some of the best studied recent dike-induced swarms, share some common features: (1) The vast majority of the earthquakes are normal faulting or strike slip, and often oblique mechanisms or earthquakes of both types are present; 2) the *T* axes of the earthquakes are mostly perpendicular to the dikes; and (3) the *P* axes have a wider variability. These observations inspire questions about the interplay between tectonic and dike-induced stresses in generating the observed FMs either dominated by normal or strike-slip faulting.

In general, the observed geometries and variety of FMs are more complex than the 2-D models available to explain them so that a generalization of geometries and models as done by *Hill* [1977] and *Rubin and Pollard* [1988] are desirable to address the observed complexities. Additional studies relating seismicity rate increases and decreases to Coulomb stress changes have been published recently [*Toda et al.*, 2002; *Hughes*, 2010; *Passarelli et al.*, 2013; *Maccaferri et al.*, 2013], but these studies did not address the observed or expected orientation of the FMs in space.

Schorlemmer et al. [2005] showed that for different focal mechanisms of tectonic earthquakes, the slope of the Gutenberg-Richter model (*b* value), which describes the relative frequency of large earthquakes over small ones, is different: thrust, strike-slip, and normal fault events have $b < 1$, $b \approx 1$, and $b > 1$, respectively. This mirrors seismogenic environments with different levels of confining stress [*Scholz*, 1968]. In volcanic areas a large variability of *b* values both in space and time is often found, with a wide range of observed values and

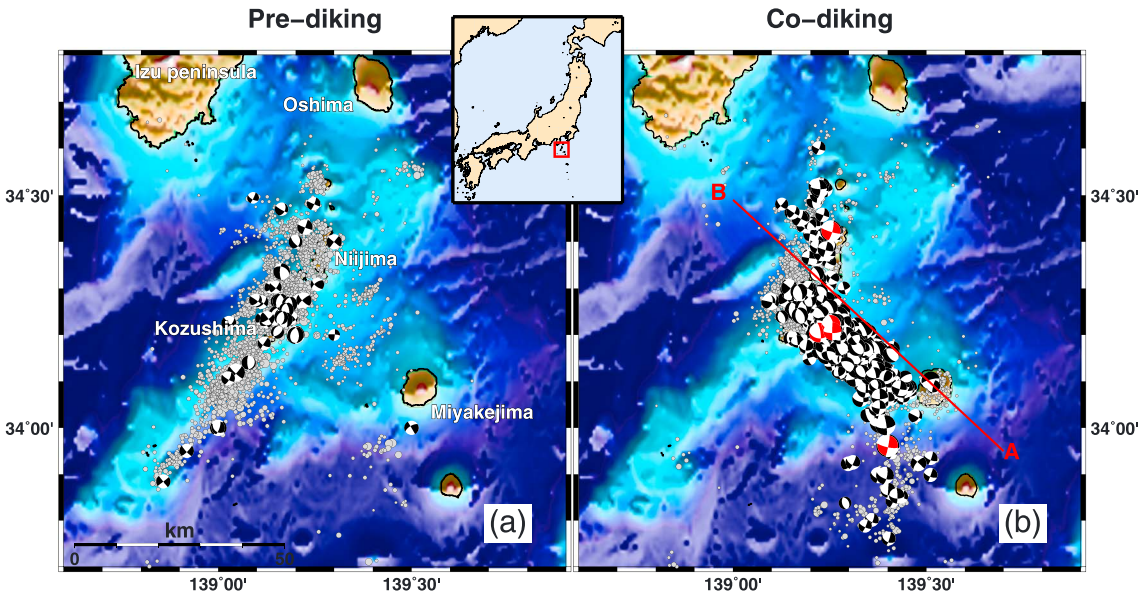

Figure 1. (a) Prediking focal mechanisms (January 1997 to 25 June 2000) from the NIED catalog. Light gray circles are epicentral locations of seismicity in the same time period from the JMA catalog. (b) Same as Figure 1a but for the period 26 June to 30 September 2000 (codiking period). Red focal mechanisms are the five $M_J > 6$ events. Inset: map of Japan with red box indicating the studied area.

significant anomalies in space and fluctuations in time. In particular, *b* values significantly larger than 1 are not rare [*McNutt*, 1996; *Wiemer et al.*, 1998; *Wiemer and Wyss*, 2002; *McNutt*, 2005; *Farrell et al.*, 2009; *Jacobs and McNutt*, 2010; *Belachew et al.*, 2011; *Shuler and Nettles*, 2012], highlighting how volcanic seismicity is often dominated by small-magnitude earthquakes. In general, the *b* value may be influenced not only by the confining stress but also by material and other stress heterogeneities, including high density of fractures [*Mogi*, 1962], weak or ductile material rheology [*Amitrano*, 2003; *Bean et al.*, 2014], limited thickness of competent rock layers [*Richardson and Jordan*, 2002; *Becker et al.*, 2010], thermal gradients [*Warren and Latham*, 1970], and high pore pressure levels [*Wyss*, 1973; *Hill et al.*, 1990; *Wiemer et al.*, 1998; *Farrell et al.*, 2009]. Often, some of these mechanisms may work in concert: pockets of high *b* values underneath volcanoes often overlap with anomalous low-velocity zones of seismic waves [*Wiemer and McNutt*, 1997; *Sanchez et al.*, 2004]. This observation is interpreted as small-size brittle failures occurring in a ductile medium with a high fracture density and permeated by fluids exsolved from magma bodies [*Murru et al.*, 1999; *Wiemer and McNutt*, 1997; *Wiemer et al.*, 1998; *Sanchez et al.*, 2004].

Here we investigate the faulting geometry and the scaling properties of the earthquakes induced by the Miyakejima dike and compare them with the faulting style expected for a penny-shaped crack model. We use data from the 2000 Miyakejima intrusion in Japan, for which a large catalog of FMs is available. We group earthquakes with similar focal mechanisms by applying a clustering procedure, describe the group properties of the different families, and discuss the oblique FMs in terms of a 3-D model of dike-induced stress changes. Finally, we analyze the frequency-magnitude distribution for the earthquakes as a function of their FMs and discuss the results in terms of faulting geometry, stress levels, and material heterogeneities.

2. Tectonic Setting and Chronology of the Intrusion

The Izu Islands chain lies on the Philippine Sea plate 100 km west of the triple junction of the Eurasian, Pacific, and Philippine Sea plates [*Stein et al.*, 2006]. The rather complex tectonic setting is dynamically very active: the Pacific plate is subducting underneath the Philippine Sea plate with an annual rate of 8 cm/yr in the WNW direction, and the Philippine Sea plate moves northwestward at about 3 cm/yr, subducting underneath the Eurasian plate from the Suruga trough and the Sagami trough [*Ozawa et al.*, 2004; *Stein et al.*, 2006].

The area where the 2000 dike intruded lies in the northern part of the Izu archipelago NW of Miyakejima and SE of Kozushima and Niijima (Figure 1). Most epicenters preceding the dike intrusion (January 1997 to 25 June 2000) located by the Japan Meteorological Agency (JMA) align NE-SW extending from Niijima to nearly 40 km

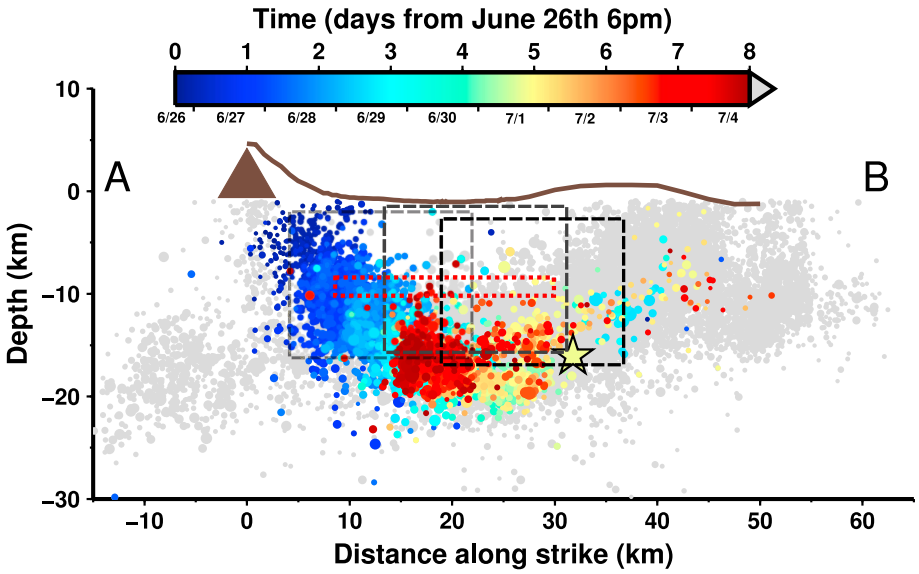

Figure 2. Codiking hypocenters projected on a vertical cross section along the segment AB in Figure 1b. The origin of the coordinate system is at Miyakejima [34.079°N, 139.529°E]. The data are from the JMA catalog. Days since 26 June at 18:00 JST are color coded, marker size scales with magnitude. The large triangle indicates the position of Miyakejima volcano. The solid line is the topography/bathymetry along the segment AB in Figure 1b magnified by a factor of 5. The large star is the $M_l = 6.5$ earthquake occurred on day 4.8 since the onset of the swarm. Light gray circles indicate all seismicity after 4 of June (day 8 since the dike intrusion start) and for the whole codiking period as defined in the text. The dotted red box is the dike geometry of *Ozawa et al.* [2004] used to model dike-induced deformation. Dashed boxes are dike geometries of *Ito and Yoshioka* [2002] and light gray, dark gray, and black colors refer to phases 1, 5, and 8, respectively (see *Ito and Yoshioka* [2002], for more details).

SW of Kozushima (Figure 1a, light gray circles). More tectonic structures SE of Kozushima and Niijima and SSW of Miyakejima are also visible.

On 26 June 2000 at approximately 18:00 (Japan standard time) a cluster of earthquakes struck at a depth of about 3 km underneath Miyakejima [*Nakada et al.*, 2005]. In the first 3.5 h the seismicity was located within the SW quadrant of Miyakejima showing ENE-WSW propagation [*Uhira et al.*, 2005]. Then, the seismicity migrated toward NW, in the direction of Kozushima and Niijima for nearly 5 days (Figure 2). The NW-SE emplacement of the dike is broadly consistent with the NE-SW extensional tectonics inferred for the intrusion area [*Ukawa*, 1991; *Fukuyama et al.*, 2001]. On day 4.8 from the onset of the seismic swarm, a $M_l = 6.5$ event occurred near the propagating tip (Figure 2). (see other examples of large dike-triggered earthquakes by *Buck et al.* [2006] and *Passarelli et al.* [2013]). After that, the dike stopped propagating and continued inflating and possibly extending vertically, as demonstrated by increased displacements at the GPS stations at Miyakejima, Kozushima, Niijima, and on the Japan mainland [*Ozawa et al.*, 2004; *Nakada et al.*, 2005; *Yamaoka et al.*, 2005; *Hughes*, 2010]. The seismic activity continued with a high rate for nearly 3 months including five $M_l > 6$ earthquakes [*Ozawa et al.*, 2004] (Figure 1b). Three struck approximately where the dike tip stopped, while the other two occurred in the northern and southern branches of the seismicity [*Uhira et al.*, 2005; *Wright and Sakai*, 2005].

Several studies have focused on modeling the sources of deformation [*Ito and Yoshioka*, 2002; *Irwan et al.*, 2003; *Ozawa et al.*, 2004; *Yamaoka et al.*, 2005; *Hughes*, 2010]. The source parameters for the dike, however, are not well constrained due to the unavoidably nonoptimal spatial coverage of the GPS stations. *Irwan et al.* [2003] modeled the deformation recorded during the first 12 h by the local GPS network. They found a satisfying match to the data by assuming a small NE-SW oriented dike, later deflating into a NW-SE oriented dike which caused a submarine eruption in the morning of 27 June. When inverting the entire deformation through to September 2000 [*Nakada et al.*, 2005], more sources are needed: a large NW-SE oriented dike, a deflating Mogi source underneath Miyakejima, and one or more creeping faults in different areas [*Ito and Yoshioka*, 2002; *Ozawa et al.*, 2004; *Yamaoka et al.*, 2005; *Hughes*, 2010]. Almost all dike models dip vertical except for one of *Ito and Yoshioka* [2002] who introduce a subvertical dike (dip ≈ 100°). In Figure 2 we report the two different dike geometries used by *Ito and Yoshioka* [2002] and *Ozawa et al.* [2004] in their time-dependent inversion

of deformation data. We refer to these models later on in the paper when we discuss the spatial distributions of FMs of the Japan National Research Institute for Earth Science and Disaster Prevention (NIED) catalog.

3. Focal Mechanism Data

The primary data set for the present study is the double-couple FM catalog by the Japan National Research Institute for Earth Science and Disaster Prevention (NIED). We use FMs in the period January 1997 to September 2000 and the area delimited by [138.6°, 139.9°]E and [33.7°, 34.8°]N with hypocentral depths between 0 and 30 km. The extracted catalog consists of a total of 1499 events with M_w >3. A grid spacing of 10^{-4}° and 3 km in the horizontal and vertical directions, respectively, is used in the inversion procedure. The FM catalog does not include a nominal uncertainty associated with the hypocentral locations of the inverted fault planes. Errors in the locations, especially hypocentral depths, are expected to be in the order of a few kilometers.

We focus our analysis on the period from 27 June 2000 to 24 September 2000 (codiking phase) and compare it with the tectonic seismicity before the dike intrusion (January 1997 to 25 June 2000, prediking phase). During the prediking phase 46 FMs are available, shown in Figure 1a. The FMs show predominantly strike-slip mechanisms with a small, variable normal component. None of the events have pure reverse FMs, consistent with the general extensional tectonics of the area [*Ukawa*, 1991; *Ida*, 2009]. Pure normal faulting events striking predominantly N-S are confined in a small region between Kozushima and Niijima; see Figure 1a.

For the codiking period, the catalog contains 1453 FMs, as in Figure 1b. A broad range of FMs were found, but mostly FMs are oblique with strike-slip mixed to normal. Pure normal faulting FMs are present, while pure thrust ones are absent.

4. Clustering Analysis

We classify the seismic events according to their FMs by using the approach by *Cesca et al.* [2014] and *Maghsoudi et al.* [2014]. Similar double-couple solutions are grouped based on the similarity of the normalized Kagan angle [*Kagan*, 1991, 1992]. The result of the clustering procedure depends on two parameters (N_{min}, ϵ) that affect the number and homogeneity of the identified clusters. For each cluster, a barycentric focal mechanism is identified by minimizing the sum of its distances (Kagan angles) from the events within a cluster. This clustering approach is preferable to a simple classification based on single fault plane angles (i.e., rake) because it accounts for the combined variation of strike, dip, and rake angles (or, alternatively, *P*, *T*, and *B* axes). Moreover, the algorithm requires no assumption on the true fault plane orientation.

We apply the clustering procedure separately to the prediking and codiking FMs, setting N_{min} and ϵ to 5 and 0.95, respectively. Results of the clustering are reported in Table 1. Out of a total of 46 FMs in the prediking phase, 20 are unclassified while the remaining 26 events are classified in four clusters (Figure 3).

For the codiking phase the clustering algorithm groups 1000 FMs into 13 clusters, while 453 remain unclassified (Table 1 and Figure 4). The number of events within a cluster varies between 5 and 565. To obtain more robust statistical results, we focus our analysis on the four largest clusters, with more than 30 events (Table 1).

Within the four clusters of prediking FMs, one includes predominantly normal faulting and three include predominantly strike-slip events differing in strike or dip (Figures 3a and 3b). The *T* axes of all earthquakes (clustered and unclustered) are approximately EW oriented (Figure 3c). The orientations of the *P* and *B* axes vary over the entire range of possible values compatible with a fixed *T* axis. This is consistent with the predominantly extensional tectonics of the area, resulting in a lack of reverse faulting events. All *P*, *T*, and *B* axes of the strike-slip clusters are tightly clustered, suggesting that the strike-slip seismicity mainly occurs on subparallel fault planes with possible orientations NW-SE and NE-SW. The *T* axes of the normal faulting family are very similar to the *T* axes of the strike-slip cluster. Since the normal faulting events striking NS are located within a relatively small area off the east shore of Kozushima, the rotation of the axes is likely governed by a local effect that perturbs the balance of σ_1 and σ_2, while σ_3 remains stable. On a strike-rake plot (Figure 3d) the events align on an oblique segment, indicating a correlation between strike and rake resulting from a stable *T* axis and unstable *P* and *B* axes.

Both the patterns of the epicenters and the FMs changed significantly during the codiking phase (Figure 4). The *T* axes of all clusters are rotated with respect to the prediking phase (Figure 4b). The tight clustering of the *T* axes is maintained in the codiking phase, but now the *T* axes are oriented NE-SW, perpendicular to the dike

Table 1. Number of Events and Barycentric Focal Mechanisms for Recognized Clusters[a]

Number of Events	Strike[b]	Dip[b]	Rake[b]	R-G-B Code	Color Name
		Prediking			
8	133.0	90.0	−149.0	0-100-0	Dark green
7	358.0	61.0	−103.0	139-61-139	Magenta
6	318.0	90.0	154.0	84-255-159	Sea green
5	42.0	90.0	−6.0	139-62-47	Dark coral
		Codiking			
565	363.0	88.0	−24.0	0-0-250	Blue
279	162.0	71.0	−50.0	255-0-0	Red
52	99.0	84.0	−164.0	0-255-255	Cyan
34	309.0	59.0	−93.0	255-140-0	Dark orange
18	154.0	81.0	−27.0	165-42-42	Brown
12	297.0	53.0	−104.0	142-35-35	Firebrick
7	141.0	52.0	−80.0	160-82-45	Sienna
7	288.0	54.0	−118.0	92-64-51	Dark brown
6	93.0	70.0	−151.0	72-61-139	Dark slate blue
5	302.0	54.0	−117.0	255-127-0	Coral
5	288.0	88.0	172.0	95-159-159	Cadet blue
5	283.0	62.0	−137.0	139-37-0	Orange red
5	295.0	67.0	−119.0	255-20-147	Deep pink

[a]In the last two columns the color code used in Figures 3 and 4 is indicated.
[b]Barycentric values for stike, dip, and rake for each cluster. They are obtained by minimizing the sum of distances (Kagan angles) of all events within the individual cluster.

strike (Figure 4c). The *P* and *B* axes, instead, take all possible orientations given the common *T* axis, reflecting the large variability of focal mechanisms from strike-slip to normal faulting (Figure 4c).

Two of the four main clusters have predominantly strike-slip barycentric FMs, and two have predominantly normal faulting. The *P* and *B* axes for the predominantly strike-slip events are not distributed around a specific orientation as in the prediking phase but vary encompassing all possible orientations from the horizontal to the subvertical. On a strike-rake plot, most events align on stripes similar to the prediking seismicity except that the stripes are translated vertically to reflect the rotation of the *T* axis and that the events cover densely the full range of oblique mechanisms between pure strike-slip and normal faulting (Figure 4d). The pure normal faulting earthquakes (rake = −90°) strike exactly parallel to the dike (horizontal dashed line, 310°N according to the dike models published by *Ozawa et al.* [2004]). The pure strike-slip mechanisms (rake equal to 0° and ±180°) strike approximately 10° and 250°, about ±60° from the dike strike.

The most populated cluster (in blue) is composed of 565 events (Figures 4 and 5). They are mainly strike slip with variable normal component, and only few have a thrust component. They strike ±70° around the dike strike direction and dip from 30° to 90°. Four out of the five largest events registered belong to this cluster. The pure strike-slip, cyan cluster (Figures 4 and 5) contains 52 events, including the northernmost $M_l > 6$.

The oblique normal faulting mechanisms shown in red in Figure 4 are the second most populated cluster, with 279 events. They have large normal faulting component, dip between 30° and 80°, and strike subparallel to the dike. Their strike-slip component is with rake angle between −30° and −70° or between −110° and −170° depending on the focal plane considered. The pure normal faulting events (orange cluster) strike parallel to the dike and are located approximately in the middle of the seismic cloud (Figures 4 and 5).

The predominantly strike-slip events (cyan and blue clusters) start earlier in the sequence than the normal faulting cluster; events are distributed in the whole area lit up by the seismicity (Figures 4 and 5). The mechanisms with predominantly downdip normal component (red and orange clusters) are more confined in space around the final location of the dike (black/gray segments and red segment in Figures 5b and 5e) and at shallow depth (Figure 6). They activated about 2 days after the propagation onset and are less abundant during the propagation (Figure 5).

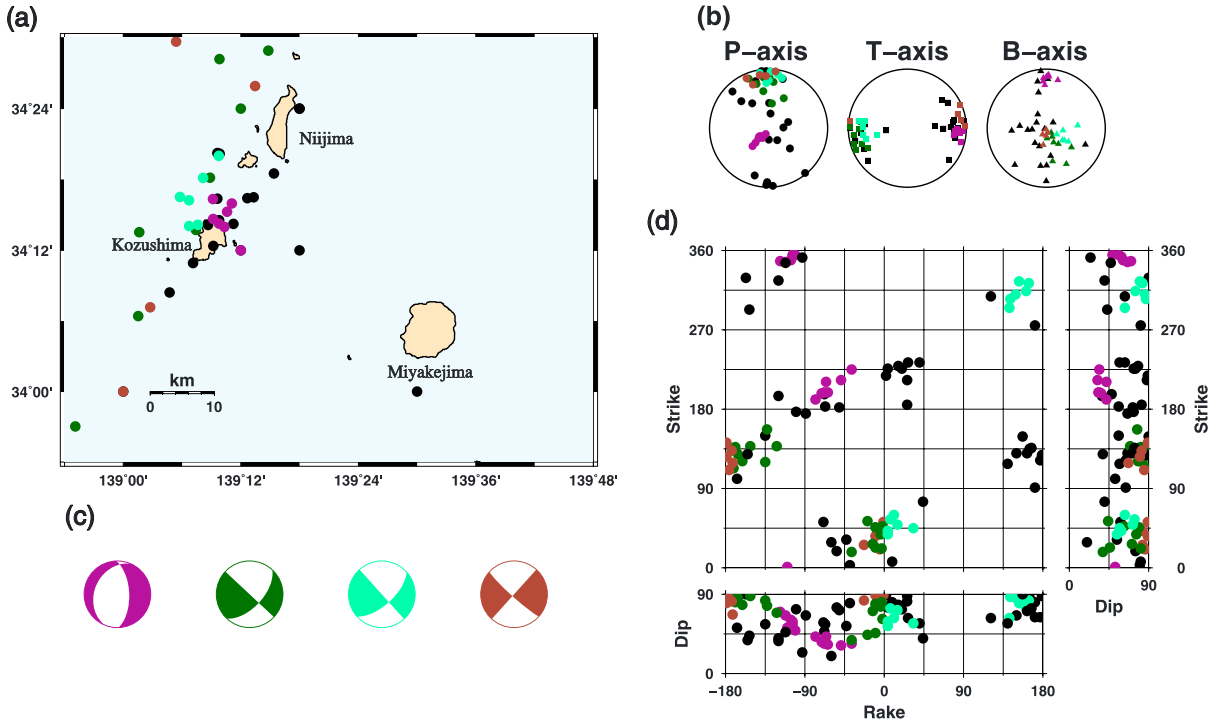

Figure 3. (a) Map view of the results of the clustering procedure for prediking FMs. Colors indicate different families; black circles are unclustered events. (b) *P*, *T*, and *B* axes for the earthquakes. (c) Barycentric FMs for the four identified clusters. (d) Strike, rake, and dip distribution for the two focal planes of the FMs in the NIED catalog.

5. Coulomb Stress Change Analysis

In crustal deformation studies dikes are often modeled as rectangular opening dislocations. This choice has at least two big advantages: flexible analytical solutions for the stress and displacements fields in a half-space [*Okada*, 1992] and a low number of free parameters. Such an approach, however, is not helpful when studying the FMs of the induced earthquakes, as they originate from the stresses near the dike borders, which are very sensitive to the geometry of the dike.

We now calculate the dike-induced Coulomb stress change (ΔCFS) with the purpose of showing that by taking into account a more realistic 3-D shape, we can explain the distribution of FMs, with particular regard to the oblique mechanisms. We do not attempt to model the Miyakejima dike because the dike enlarged significantly throughout the emplacement process and its shape is not well constrained by deformation studies. We instead design a generic model for a large dike intrusion with size similar to the 2000 Miyakejima dike by building a boundary element model for a pressurized dike of elliptical shape in a homogeneous half-space (Figure 7a). The effect of the loading due to the volcanic islands is not considered, nor are the external tectonic stresses which we assume to be negligible in the near field. We subdivide the dike ellipse, of semiaxes 10 km × 6 km, in rectangular tensile dislocations of sides 1 km × 1 km [*Okada*, 1992], prescribing an overpressure of 5 MPa at the center of each dislocation and inverting for the required opening of each patch [*Crouch and Starfield*, 1983].

The ΔCFS, calculated on optimally oriented planes, on a horizontal cross section through the center of the dike (Figure 7b, calculated in position A in Figure 7a) is negative at the sides of the dike, where compressional stresses are strong, and positive in the tip region (Figure 7b). Two lobes with high Coulomb stresses are visible at the side of the tip. These lobes are expected to host strike-slip earthquakes (due to symmetry, the deformation will be approximately plain strain). The ΔCFS on a vertical cross section through the center of the dike (Figure 7c, calculated in position B in Figure 7a [see also *Rubin and Pollard*, 1988]) with our choice of parameters is more intense than the ΔCFS on the horizontal cross section. This is due mainly to the fact that the dike is longer than higher so that the same pressure will cause a larger curvature at the upper and lower edges. The free surface has the effect to focus the stresses and modify the shape of the two lobes of

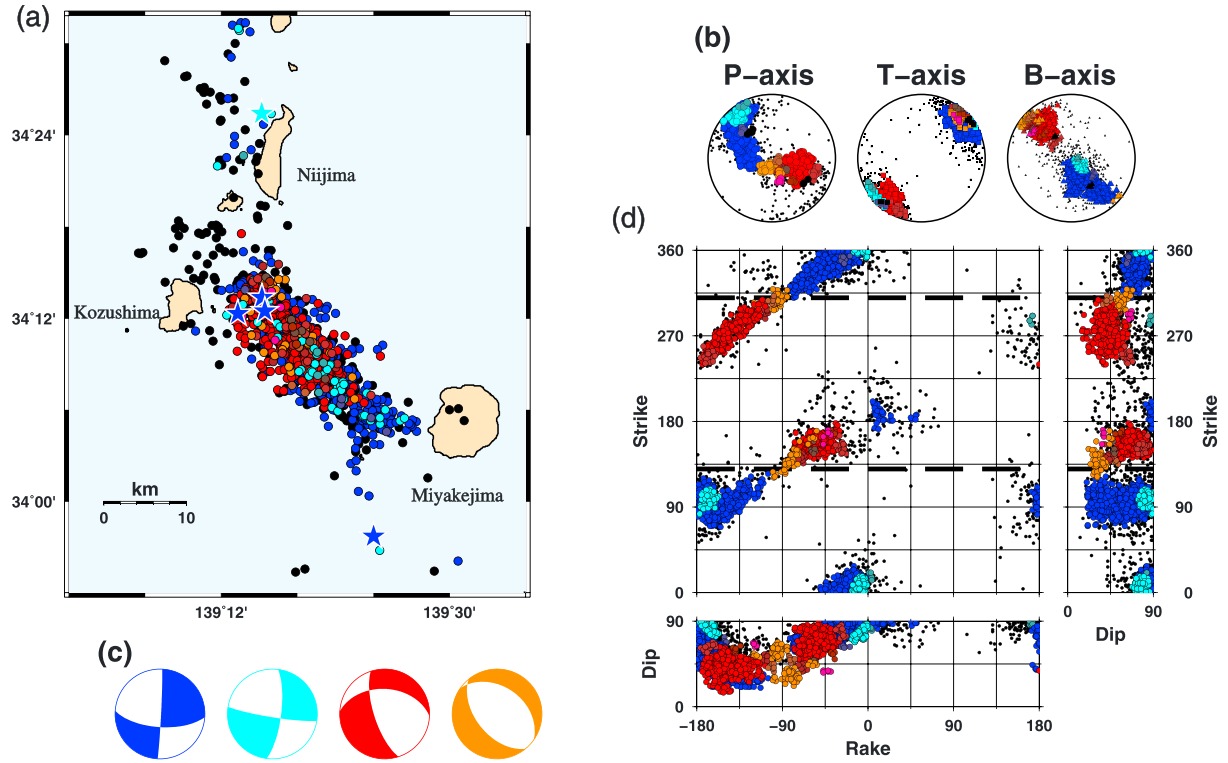

Figure 4. (a) Map view of the results of the clustering procedure for the codiking FMs. Color-coded circles are different clusters of FMs, and colors are reported in Table 1. Black circles are events not clustered by the algorithm. Stars indicate $M_l > 6$ events, colored according to which cluster they belong to. (b) *P*, *T*, and *B* axes for the FMs. (c) Barycentric FMs for the four families containing more than 30 events. (d) Strike-rake, dip-rake, and dip-strike plots and both focal plane solutions for each event are plotted. Dashed lines represent the dike strike angle according to *Ozawa et al.* [2004].

high Coulomb stresses at the side of the tip. This will cause the normal faulting forming graben structures often observed in correspondence of shallow dikes [*Hill*, 1977; *Rubin and Pollard*, 1988; *Pallister et al.*, 2010]. We observe that along the entire dike border (see, for example, position C in Figure 7a) there will be a similar stress concentration and two lateral lobes of high Coulomb stress.

The problem of predicting the 3-D surfaces where faulting occurs is nontrivial, and no models are current available. The orientation of the potential shear fractures is determined by maximizing the Coulomb stress for a given principal stresses configuration. Two shear surfaces are obtained at each location. How the fracture will propagate into the host rock depends on which of the two surfaces will be taken by the rupture surface and cannot be determined by the Coulomb stress only. However, we know from geological investigation that dikes produce faulting on graben structures with dip angles varying between 40 and 60° from the dike plane. The intersection of this graben surfaces with the 3-D Coulomb stress field produced by an elliptical dike, will give two curved surfaces where it is likely to host most faulting events. This will be a hyperboloid-like surface as in Figure 7d departing from the dike border. These surfaces will host oblique FMs (oblique slip on oblique planes).

This theoretical picture extends the 2-D models by *Hill* [1977] and *Rubin and Pollard* [1988]. It is consistent with the FM catalog for the Miyakejima dike: the model predicts normal faulting events striking parallel to the dike, strike-slip FMs striking at about 45–60°, and the whole range of intermediate FMs between those two types. The model also expects normal faulting shallower (and possibly deeper) than strike-slip mechanisms at any given time. For the Miyakejima dike, normal faulting events are confined at shallower hypocentral depths (Figure 6).

6. Frequency-Size Distributions of the Clustered Families

To study the scaling properties of the dike-induced earthquakes as a function of their FM (and therefore stress) and of the 3-D dike geometry, we collect the four codiking clusters into two families, one predomi-

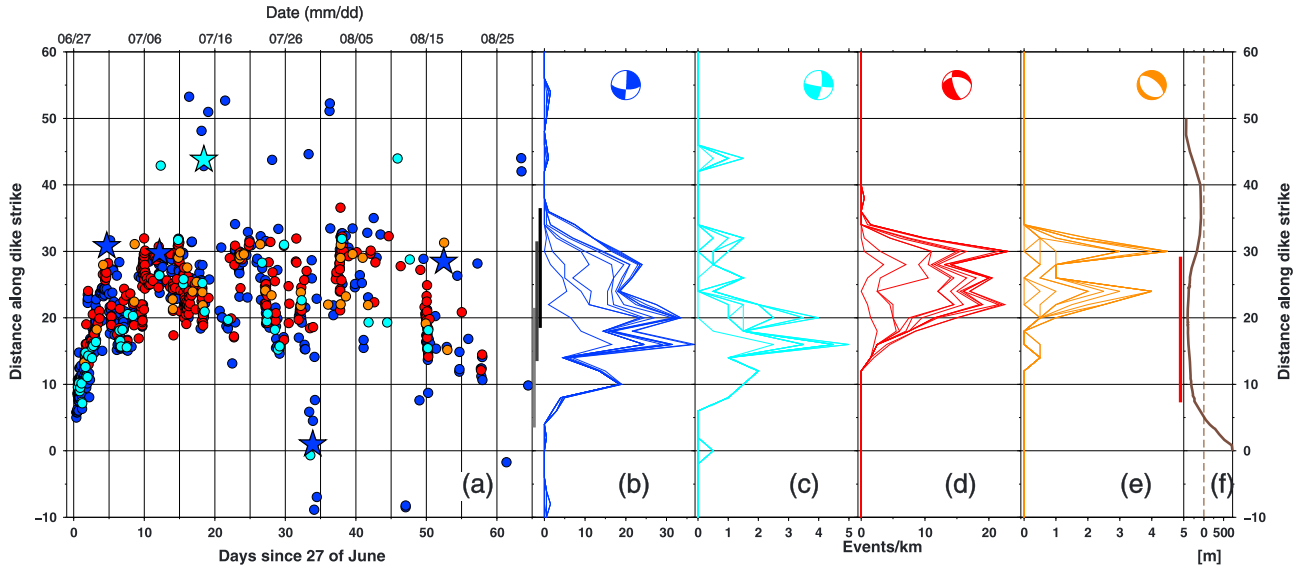

Figure 5. (a) Distance from Miyakejima volcano versus time of occurrence for the events in the codiking phase. The colors refer to the four codiking clusters families as in Figure 4c. Distances are calculated along the AB segment in Figure 1 with origin in the Miyakejima as in Figure 2. Stars indicate $M_J > 6$ events. Seven events that occurred after day 65 are left out, specifically three unclustered, two from the blue family, one from the cyan family, and one from the red family. (b–e) Cumulative density of events per kilometer along the distance from Miyakejima (AB segment in Figure 1b, binning size is 2 km) for the four selected clusters. The barycentric FM is indicated in each panel as beach ball. Each line represents the cumulative number of events/km in 5 day time lags from 27 June 2000. In Figures 5b and 5e, the vertical thick bars are dike models as reported in Figure 2. (f) The topography/bathymetry is plotted along the AB segment in Figure 1a.

nantly strike-slip (red and cyan clusters in Figure 4, 617 events) and one predominantly normal faulting (red and orange clusters in Figure 4, 313 events). We fit the Gutenberg-Richter model (GR) [*Gutenberg and Richter*, 1944] to the observed frequency-magnitude distribution to both data sets. GR is defined as the number of events exceeding magnitude M is given by $N(M^* > M) = 10^{a-bM}$, where a is the earthquake productivity and b gives the relative proportion of small to large events.

We calculate the b value and magnitude of completeness, M_c, with the stability method of *Cao and Gao* [2002] modified by *Woessner and Wiemer* [2005]. Uncertainties on the parameters are 1 standard deviation of the empirical distribution of b values and M_cs resulting from bootstrapping with replacement the original catalog 1000 times [*Woessner and Wiemer*, 2005] (see Figure 8).

For the strike-slip clusters we find $b = 1.1$, with a satisfactory fit across all magnitudes above M_c, including the largest events (Figure 8a). Hence, the statistics of the strike-slip family induced by the Miyakejima dike is similar to that of pure tectonic earthquakes calculated on the global scale [i.e., *Frohlich and Davis*, 1993]. We find the same value $b = 1.1$ for the normal families. However, the best fit curve matches the observed distribution rather poorly (Figure 8b). The distribution shows a marked roll-off on its right-hand tail associated

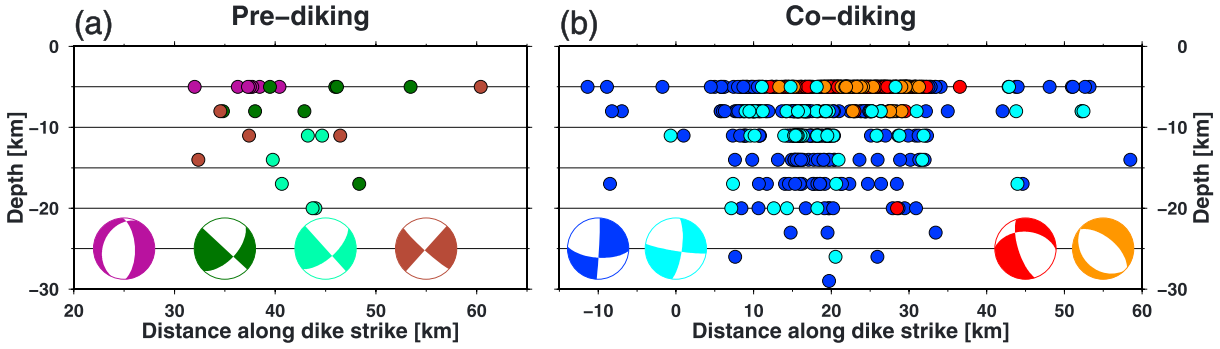

Figure 6. Depth distribution of FMs along the profile AB in Figure 1 with origin at Miyakejima for (a) the prediking and (b) the codiking phases. Colors indicate the cluster families and barycentric mechanisms as in Figures 3 and 4. The leveled distribution of depths results from the NIED inversion procedure with fixed grid space of 3 km in depth.

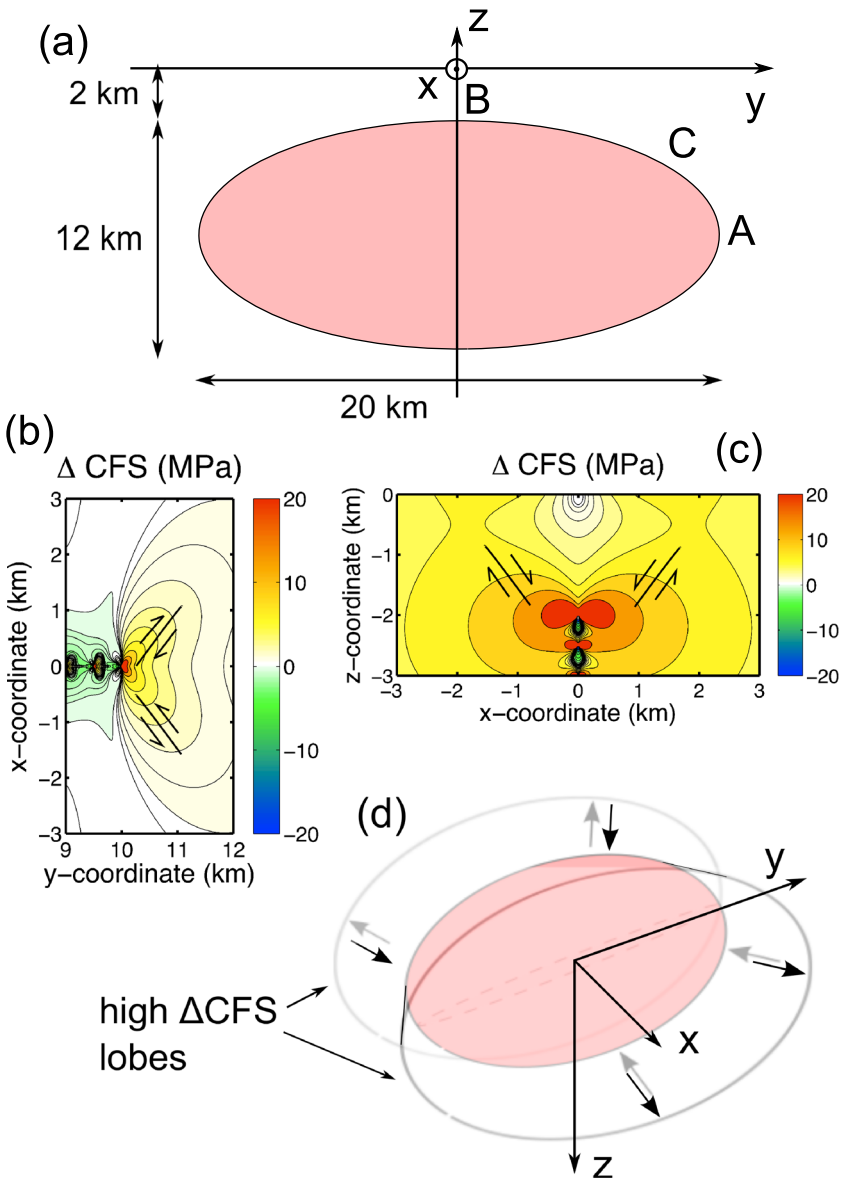

Figure 7. (a) Numerical dike model and coordinate axes. The elliptical dike surface is subdivided in 1 × 1 km patches. An overpressure of 5 MPa is prescribed at the center of each patch. (b) Horizontal cross section of modeled Coulomb stress change on optimally oriented faults. The dike length is 20 km; only the tip region is shown here. (c) Vertical cross section of the Coulomb stress change. The vertical extension of the dike is 12 km, only the tip region and the free surface are shown here. The singularities in the stress maps shown in Figures 7b and 7c are due to the chosen discretization of the dike model. (d) Perspective view (including coordinate axes) of the location and orientation of fault planes (oblique surfaces departing from the dike border) favored by the dike stresses. The elliptical dike surface is pink shaded. Arrows indicate the sense of slip.

to a lack of $M > 5.5$ earthquakes. This prevents a good fit; using a different method, giving more weight to the large-magnitude events would have resulted in a high b value. The data could be fitted by a piecewise linear function with two different slopes [e.g., *Legrand et al.*, 2004]. We do not perform such a fit because of the limited magnitude range available and because it cannot give us additional insight into the mechanics behind the observations.

Instead, we validate the departure of the data from the GR relationship by using the Goodness-of-fit method to infer M_c and b value simultaneously [*Wiemer and Wyss*, 2000; *Woessner and Wiemer*, 2005]. This method is based on the statistical comparison of the empirical distribution of the data and the GR model by varying the cutoff magnitude. The minimum M_c and associated b value explaining more than 90% of the data are chosen

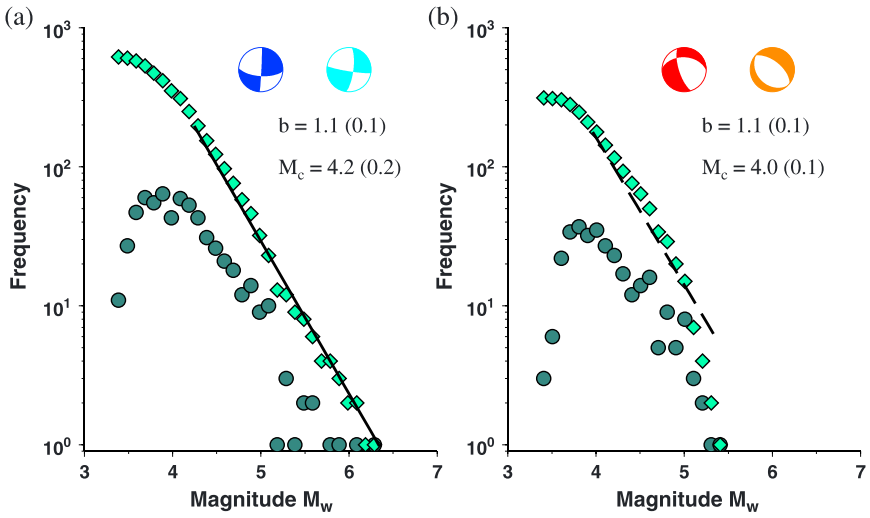

Figure 8. (a) Frequency-magnitude distribution for the strike-slip clusters represented by their barycentric beach balls. Dark green circles and light green diamonds are the absolute and cumulative frequency, respectively; the solid line is the best fit curve. The inference for *b* value and M_c are indicated in the figure and in parentheses are errors. (b) Same as Figure 8a but for normal faulting events. The dashed line represents the best fit GR curve estimated with the stability method by *Cao and Gao* [2002] modified by *Woessner and Wiemer* [2005].

as best fit parameters [*Woessner and Wiemer*, 2005]. We perform increments of the cutoff magnitude until a minimum number of 50 events is available for the inference. The increase of the *b* value with M_c indicates a poor fit of the model for the largest magnitudes (Figure 9).

As a final test, we recalculate the statistics by grouping the entire FM catalog purely by the rake angle of the earthquakes, considering the entire FM catalog. We group the events into two sets: (1) All the FMs with a dominant normal faulting component and (2) all the remaining ones. To do so, we select varying windows for the data: we start forming the normal faulting group by collecting FMs with rake [−70, −110]° and then iteratively extend it at both sides by increments of 10° [*Schorlemmer et al.*, 2005] until we reach [−20, −160]°. We find that the departure from the fit to a simple GR relation with a significant lack of large earthquakes appears for rake

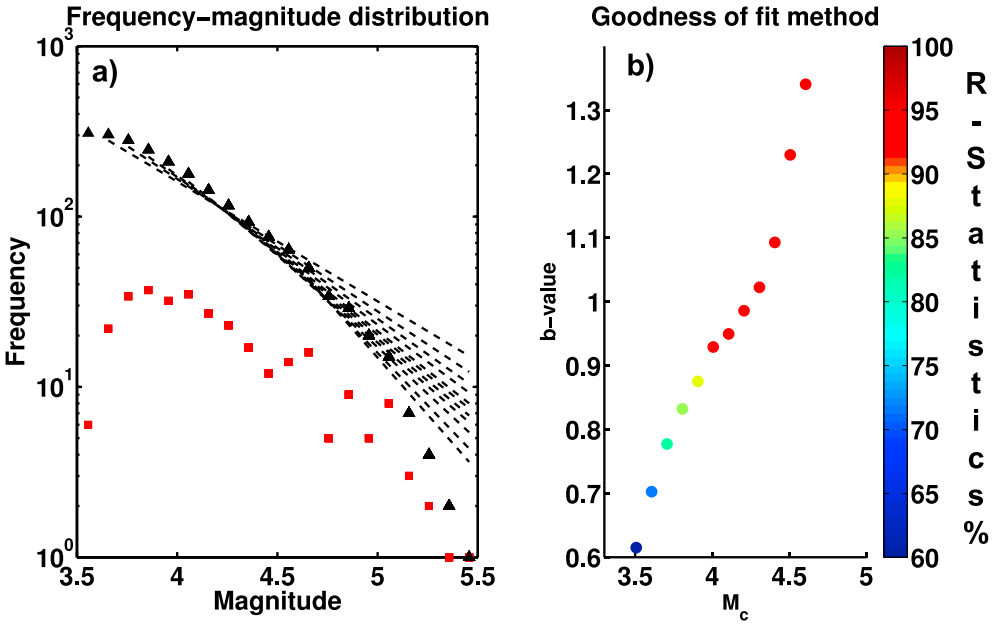

Figure 9. (a) Frequency-magnitude distribution of normal faulting events (red and orange clusters) as in Figure 8b. The dashed lines are GR fits for 0.1 increments of M_c. (b) M_c versus *b* values and color-coded R_{stat} as discussed in the text.

angles between [−30, −150]° confirming the results presented above. Conversely, the remaining strike-slip mechanisms are well fitted by the GR model with a *b* value = 1.1.

7. Discussion

7.1. Volcanotectonics

The dike intrusion caused a significant change both in the spatial distribution of the epicenters and in the direction of the FM principal axes.

The area SW of Kozushima was very active before the intrusion, and it became later completely silent (Figure 1). *Hughes* [2010] calculated the Coulomb stress changes induced by the dike on left-lateral strike-slip receiver faults, showing that the dike induced a negative Coulomb stress change on the area and explaining the post-diking lack of seismicity SW of the dike. A similar abatement of seismicity due to a large dike injection was reported for the Tjörnes Fracture Zone, North Iceland [*Stefansson et al.*, 2008], and attributed by [*Maccaferri et al.*, 2013] to a strong stress shadow induced by the 1975–1984 Krafla rifting episode.

The area NE of Kozushima was active both in the prediking and codiking phases, but the orientation of the stress axes in the two period of times differ significantly, with a rotation of the *T* axes of about 40°–50°. Figures 3b and 4b show that not only the rake changed with the dike intrusion but also all couples strike dip (at least for the large earthquakes for which a FM could be inverted), suggesting that none of the prediking geometries was activated in the codiking phase. In order to explain the distribution of FMs in the codiking phase, a wide range of preexisting structure orientations must be available (this may be quite common for volcanic areas, where stresses and materials are heterogeneous). It appears that the dike-induced stresses overprinted efficiently the regional stresses in this area and triggered earthquakes encompassing the entire range of optimally oriented focal planes.

The area between Miyakejima, Kozushima, and Niijima was relatively inactive before the intrusion, except for some seismicity halfway between Miyakejima and Kozushima, aligned on NE-SW trends [*Fukuyama et al.*, 2001] (Figure 1). The only focal mechanism available for that area has a NE-SW *T* axis (Figure 1). The stress field within the Izu block has been modeled by *Ukawa* [1991], showing a fan-shaped orientation around N-S direction of the *P* axes in the northern part of the Izu block (Izu Peninsula). In the emplacement area, the inferred stress field has an average NW-SE *P* axis and NE-SW extension. The final geometry of the 2000 dike intrusion confirms the prediction of the model presented by *Ukawa* [1991].

This could also explain the rotation of the dike in the first hours of the emplacement [*Irwan et al.*, 2006]. Initially, the dike orientation was likely governed by local stress field dominated by the topography of Miyakejima. The radial distribution of fissures on the volcano flank [*Ida*, 2009] is consistent with the volcano load dominating over the regional stresses [*Dahm*, 2000; *Maccaferri et al.*, 2011]. After that, the dike entered the regional controlled NE-SW extension regime and rotated perpendicular to it.

7.2. Coulomb Stress Model and Focal Mechanisms

Previous FM inversions for dike-induced earthquakes revealed either prevailing normal faulting or prevailing strike-slip mechanisms and unexplained oblique focal mechanisms (see section 1). According to our model, oblique mechanisms occur due to oblique stress concentrations generated where the curved border of the dike is inclined. Long shallow dikes that have propagated laterally in rifts, with no significant preexisting strike-slip fault zone on their path, generate predominantly normal faulting earthquakes and a few smaller magnitude strike-slip earthquakes at the propagating tip. Ascending deep dikes generate many predominantly strike-slip earthquakes along vertical sides and a few pure normal faulting at the upper portion of the edge.

The intense stress changes due to large dikes may mask or even efficiently overprint the tectonic stresses and induce a mix of normal faulting, strike-slip, and oblique mechanisms, the latter located close to the curved borders of the dikes. This conceptual model is consistent with and extends previously proposed models [*Hill*, 1977; *Rubin and Pollard*, 1988].

The Miyakejima dike offers a great opportunity to test such a 3-D model due to the magnitude of the induced earthquakes, the quality of the observations, the relative complexity of the propagation phase, and the existence of a previously active fault zone intersecting the dike path. As mentioned above, the stresses induced by the large Miyakejima dike prevailed over the prediking stresses, and the dike-induced optimally oriented faults according to the 3-D Coulomb stress pattern. Other diking events in stronger tectonic settings, such

as in rift segments in Iceland or Ethiopia, may have been less efficient in overprinting the tectonic stresses. This interpretation may explain why normal faulting mechanisms dominated during dike intrusions there [*Belachew et al.*, 2013; *Shuler and Nettles*, 2012].

Since our model is based on the assumption of pure opening on the dike, it cannot explain observations for dikes with a significant shear component on the dike plane. A significant shear component was inverted from geodetic data associated with a 50° dipping 2007–2008 Kverkfjöll dike intrusion (North Volcanic Zone, Iceland) [*Hooper et al.*, 2011]. The dike likely propagated obliquely in a complex stress field influenced by ice cap melting following the end of the last ice age. *White et al.* [2011] found that most hypocenters were confined on a single plane. The simplest interpretation is therefore that the dike intruded into a preexisting, tectonically preloaded fault, and that the fault plane solutions of the induced earthquakes reflected the shearing process on this fault while the dike was advancing.

7.3. Departure From the Gutenberg-Richter Scaling

The scaling properties of earthquakes are influenced by the level of confining stress and correlate with the faulting style. An anticorrelation between confining stress and *b* value for different rocks was found by *Scholz* [1968] and confirmed by *Schorlemmer et al.* [2005]. *Maccaferri et al.* [2013] modeled numerically the stress transferred by a large dike on the strike-slip Husavík Flatey Fault in North Iceland. They found a correlation between the intensity of the modeled compression and the *b* values for different sections of the fault: $b < 1$ for segments of the fault under compression and $b \geq 1$ for segments that underwent decompression.

For the Miyakejima dike, rather than a correlation between faulting style/stress levels and *b* values, we find a correlation between faulting style and how well the earthquakes follow the GR model. The strike-slip earthquakes are well described by the usual tectonic statistics, while the normal faulting events show a poor GR fit with a lack of $M_w > 5.5$ events, with the magnitudes in the range 3.5 to 5, sharing the same $b \approx 1$ of the strike-slip faults. The GR model has often provided an unsatisfying match to volcanic earthquakes [*Main*, 1987; *Utsu*, 1999; *Legrand et al.*, 2004; *Jacobs and McNutt*, 2010; *Bean et al.*, 2014]: bimodal frequency-magnitude distributions or a relative lack of larger magnitude earthquakes are often observed. Since the slope of the best fitting straight line steepens if the largest magnitude events are lacking, such observations may be often mapped into larger-than-needed *b* values.

Regardless of whether it is interpreted as a high *b* value or as a poor GR fit, a lack of the largest magnitude events in a frequency-magnitude distribution is generally explained by a limited ability to accumulate large stresses. As previously mentioned, faulting style and low confining stress are possible mechanisms behind the lack of large normal faulting events. High pore pressure may also decrease the stress threshold for rupture initiation and be a common feature in volcanic areas. Magmatic dikes are known to release fluids in the hosting rock matrix, and the intense stresses focused around the dike borders will interact with the fluids already present in the rock. Material inhomogeneity, linked to intense fracturing or weakness of the shallow crustal layers, may also decrease the likelihood that fractures will grow large.

Laboratory-based experiments on rock fracturing provide hints on the dependency of the *b* value on physical parameters and rheological properties of crustal rocks. Systematically large *b* values characterize the GR distribution of thermally induced microcracks. High spatial heterogeneities in stressed rock samples mirroring spatial variation of stress field show larger *b* value than more homogeneous rock samples [*Mogi*, 1962]. *Scholz* [1968] investigated the influence of the rheology of rocks on earthquake scaling and concluded that ductile rocks tend to have larger *b* values than brittle ones. Experiments on granite rock samples subjected to increasing confining pressure by *Amitrano* [2003] resulted in decreasing *b* values of acoustic emissions. Using of a numerical model, the author argues against the role of the confining pressure in lowering the *b* value and attribute *b* value changes to the rheological behavior (brittle versus ductile) instead. Following *Amitrano* [2003], *Bean et al.* [2014] simulated the frequency-size distribution for earthquakes induced in typical near-surface volcanic rock by uniaxial stressing. The resulting curve shows a non–power law scaling typical of ductile processes and deviates significantly from the GR relation. The curve is compared with observations of long-period earthquakes on Mount Etna and Turrialba volcanoes which show large *b* values with marked roll-off, indicating a departure of the largest events from power law scaling.

Lastly, the normal faulting events may have been limited in their dimension by the volume of the layer where they nucleated, between the dike upper edge and the surface of the Earth. The hypocentral depths of the FMs (Figure 6) show that the normal faulting events are located shallower compared to strike-slip

mechanisms. Considering the upper tip of the dike at 5 km depth with 15–20 km lateral extension as in *Ito and Yoshioka* [2002] and *Ozawa et al.* [2004], the maximum normal faulting event occurring above the entire dike length can have a rupture area of 75–150 km^2 (single patch with dipping angle 45°–60°). This corresponds to M_w = 5.7–6.2 [*Wells and Coppersmith*, 1994] and is about 0.5 magnitude points higher than the observed largest normal faulting in the catalog. In mining environments, a similar explanation (finiteness of the seismogenic layer above the mining stope) is invoked to explain a similar observed roll-off in the GR relationship for events located in specific layers [e.g., *Richardson and Jordan*, 2002; *Becker et al.*, 2010].

Most mechanisms described above involve low-stress drop fracturing, either directly because of lower stress levels, or indirectly because high stresses cannot accumulate on weak materials. The specific role played by pore pressure, crack density, quasi-ductility, or confining/transferred stress is difficult to separate in the Miyakejima case and in other situations because these factors are often correlated and may act in concert.

7.4. Conclusions

The analysis of the outstanding database of FMs accompanying the Miyakejima 2000 dike intrusion shows important insight on the interaction between diking and faulting in a tectonically active area. Our conclusions are as follows:

1. The final dike orientation and the rotation from the radial trajectory beneath Miyakejima to the final NW-SE orientation is consistent with the stress field modeled by *Ukawa* [1991] for the region between Miyakejima and Kozushima. The stresses induced by the dike significantly changed the seismicity in the area and modified the average orientation of the *P* and *B* axes.
2. We provide a 3-D conceptual model for the observed variability of FMs. Our model is a 3-D extension of available 2-D models. The model accounts for a more realistic penny-shaped geometry for the dike and provide a better representation of the stresses originating at the dike borders.
3. Strike-slip FMs occur in front of the shorter edges of a laterally propagating dike and normal faulting events crown the dike along its upper edge. The curved portion of the propagating edge of the dike is associated to oblique mechanisms. The *T* axis of the earthquakes is consistently perpendicular to the dike plane. This being fixed, the *P* and *B* axes orientations of the oblique earthquakes cover densely the transition between strike-slip and normal faulting earthquakes.
4. For the seismicity induced by the Miyakejima dike, we find no evidence for *b* values significantly larger than 1. Instead, we find that the statistics of strike-slip earthquakes matches the one of global tectonic earthquakes with a perfect GR fit and $b = 1.1$, while the statistics of normal faulting events is dominated by small to moderate earthquakes and lacks large-magnitude events. The GR model does not seem to describe satisfactorily the observed statistics for normal faulting events. Forcing a GR fit on the normal faulting events gives a *b* value significantly larger than 1, but we reckon this would be a misinterpretation due to a wrong choice of model.
5. Several physical mechanisms involving not only stress (faulting style, confining stress, and pore pressure increases) or material heterogeneity (fracturing, ductility, and weakness) but also a physical limit of the thickness of the layer where the earthquakes occur may be behind the lack of large normal faulting events and the poor GR fit. In the Miyakejima case, it is difficult to separate these effects because they are all correlated, as they all characterize the shallowest layers where the normal faulting earthquakes occur. Likely, they act in concert resulting in the strong statistical evidence we provide.

Acknowledgments

Data to support this article are from the Japan Meteorological Agency (JMA) and Japan National Research Institute of Earth Science and Disaster Prevention (NIED) which are the only owners of the data. Any request of data should be addressed directly to those institutions. Focal mechanisms from 2004 are available online at http://www.hinet.bosai.go.jp/. L.P. and E.R. were funded by the European Union through the ERC Starting grant project CCMP-POMPEI, grant 240583, and Med-Suv ERC funded project. S.C. was funded by the MINE project by the German BMBF "Geotechnologien" grant BMBF03G0737. We thank the Japan Meteorological Agency and National Institute for Earth Science and Disaster Prevention for access to the catalogs of hypocenters and focal mechanisms. We thank Francesco Maccaferri, Sebastian Hainzl, and Camilla Cattania for the fruitful discussion which helped us to clarify some of the ideas discussed in the paper. The comments by two anonymous reviewers and Associate Editor helped in improving the manuscript. Figures from 1–6 and 8 were drawn with GMT [*Wells and Coppersmith*, 1994].

References

Amitrano, D. (2003), Brittle-ductile transition and associated seismicity: Experimental and numerical studies and relationship with the *b*-value, *J. geophys. Res*, *108*(2044), 2109–2112, doi:10.1029/2001JB000680.

Aoki, Y., P. Segall, T. Kato, P. Cervelli, and S. Shimada (1999), Imaging magma transport during the 1997 seismic swarm off the Izu peninsula, Japan, *Science*, *286*, 927–930.

Bean, C. J., L. De Barros, I. Lokmer, J.-P. Métaxian, G. O'Brien, and S. Murphy (2014), Long-period seismicity in the shallow volcanic edifice formed from slow-rupture earthquakes, *Nat. Geosci.*, *7*(1), 71–75, doi:10.1038/ngeo2027.

Becker, D., B. Cailleau, T. Dahm, S. Shapiro, and D. Kaiser (2010), Stress triggering and stress memory observed from acoustic emission records in a salt mine, *Geophys. J. Int.*, *182*(2), 933–948.

Belachew, M., C. Ebinger, D. Coté, D. Keir, J. Rowland, J. Hammond, and A. Ayele (2011), Comparison of dike intrusions in an incipient seafloor-spreading segment in Afar, Ethiopia: Seismicity perspectives, *J. Geophys. Res.*, *116*, B06405, doi:10.1029/2010JB007908.

Belachew, M., C. Ebinger, and D. Coté (2013), Source mechanisms of dike-induced earthquakes in the Dabbahu-Manda Hararo rift segment in Afar, Ethiopia: Implications for faulting above dikes, *Geophys. J. Int.*, *192*(3), 907–917.

Brandsdóttir, B., and P. Einarsson (1979), Seismic activity associated with the September 1977 deflation of the Krafla central volcano in northeastern Iceland, *J. Volcanol. Geotherm. Res.*, *6*(3), 197–212.

Buck, W., P. Einarsson, and B. Brandsdóttir (2006), Tectonics stress and magma chamber size as controls on dike propagation: Constraints from the 1975–1984 Krafla rifting episode, *J. Geophys. Res.*, *111*, B12404, doi:10.1029/2005JB003879.
Cao, A., and S. Gao (2002), Temporal variation of seismic b-values beneath northeastern Japan Island Arc, *Geophys. Res. Lett.*, *29*(9), 1334, doi:10.1029/2001GL013775.
Cesca, S., A. T. Şen, and T. Dahm (2014), Seismicity monitoring by cluster analysis of moment tensors, *Geophys. J. Int.*, *196*(3), 1813–1826, doi:10.1093/gji/ggt492.
Crouch, S., and A. Starfield (1983), *Starfield AM (1983) Boundary Element Methods in Solid Mechanics*, 1st ed., George Allen and Unwin, London.
Dahm, T. (2000), Numerical simulations of the propagation path and the arrest of fluid-filled fractures in the Earth, *Geophys. J. Int.*, *141*, 623–638.
Dahm, T., S. Hainzl, and T. Fischer (2010), Bidirectional and unidirectional fracture growth during hydrofracturing: Role of driving stress gradients, *J. Geophys. Res.*, *115*, B12322, doi:10.1029/2009JB006817.
Einarsson, P., and B. Brandsdóttir (1980), Seismological evidence for lateral magma intrusion during the July 1978 deflation of the Krafla volcano in NE Iceland, *J. Geophys.*, *47*, 160–165.
Farrell, J., S. Husen, and R. Smith (2009), Earthquake swarm and b-value characterization of the Yellowstone volcano-tectonic system, *J. Volcanol. Geotherm. Res.*, *188*(1), 260–276, doi:10.1016/j.jvolgeores.2009.08.008.
Frohlich, C., and S. Davis (1993), Teleseismic b values: Or, much ado about 1.0, *J. Geophys. Res.*, *98*(B1), 631–644, doi:10.1029/92JB01891.
Fukuyama, E., A. Kubo, H. Kawai, and K. Nonomura (2001), Seismic remote monitoring of stress field, *Earth Planets Space*, *53*(10), 1021–1026.
Grandin, R., E. Jacques, A. Nercessian, A. Ayele, C. Doubre, A. Socquet, D. Keir, M. Kassim, A. Lemarchand, and G. King (2011), Seismicity during lateral dike propagation: Insights from new data in the recent Manda Hararo-Dabbahu rifting episode (Afar, Ethiopia), *Geochem. Geophys. Geosyst.*, *12*, Q0AB08, doi:10.1029/2010GC003434.
Gutenberg, B., and C. Richter (1944), Frequency of earthquakes in California, *Bull. Seismol. Soc. Am.*, *34*(4), 185–188.
Hill, D. P. (1977), A model for earthquake swarms, *J. Geophys. Res.*, *82*(8), 1347–1352, doi:10.1029/JB082i008p01347.
Hill, D. P., W. Ellsworth, M. Johnston, J. Langbein, D. Oppenheimer, A. Pitt, P. Reasenberg, M. Sorey, and S. McNutt (1990), The 1989 earthquake swarm beneath Mammoth Mountain, California: An initial look at the 4 May through 30 September activity, *Bull. Seismol. Soc. Am.*, *80*(2), 325–339.
Hooper, A., B. Ófeigsson, F. Sigmundsson, B. Lund, P. Einarsson, H. Geirsson, and E. Sturkell (2011), Increased capture of magma in the crust promoted by ice-cap retreat in Iceland, *Nat. Geosci.*, *4*(11), 783–786, doi:10.1038/ngeo1269.
Hughes, G. R. (2010), Investigations of magmatic end-members: Silicic magma chambers and mafic dikes, PhD thesis, Stanford Univ. [Available at http://purl.standford.edu/cf090yt6229.]
Ida, Y. (2009), Dependence of volcanic systems on tectonic stress conditions as revealed by features of volcanoes near Izu peninsula, Japan, *J. Volcanol. Geotherm. Res.*, *181*(1), 35–46, doi:10.1016/j.jvolgeores.2008.12.006.
Irwan, M., F. Kimata, N. Fujii, S. Nakao, H. Watanabe, S. Sakai, M. Ukawa, E. Fujita, and K. Kawai (2003), Rapid ground deformation of the Miyakejima volcano on 26–27 June 2000 detected by kinematic GPS analysis, *Earth Planets Space*, *55*(12), 13–16.
Irwan, M., F. Kimata, and N. Fujii (2006), Time dependent modeling of magma intrusion during the early stage of the 2000 Miyakejima activity, *J. Volcanol. Geotherm. Res.*, *150*(1), 202–212.
Ito, T., and S. Yoshioka (2002), A dike intrusion model in and around Miyakejima, Niijima and Kozushima in 2000, *Tectonophysics*, *359*(1), 171–187, doi:10.1016/S0040-1951(02)00510-3.
Jacobs, K. M., and S. R. McNutt (2010), Using seismic *b*-values to interpret seismicity rates and physical processes during the Augustine 2005–2006 pre-eruptive earthquake swarm, in *The 2006 eruption of Augustine Volcano, Alaska*, edited by J. Power, M. Coombs, and J. Freymueller, U.S. Geol. Surv. Prof. Pap., 1769, 59–83. [Available at http://pubs.usgs.gov/pp/1769/chapters/p1769_chapter03.pdf.]
Kagan, Y. (1991), 3-D rotation of double-couple earthquake sources, *Geophys. J. Int.*, *106*(3), 709–716, doi:10.1111/j.1365-246X.1991.tb06343.x.
Kagan, Y. (1992), Correlations of earthquake focal mechanisms, *Geophys. J. Int.*, *110*(2), 305–320, doi:10.1111/j.1365-246X.1992.tb00876.x.
Keir, D., et al. (2009), Evidence for focused magmatic accretion at segment centers from lateral dike injections captured beneath the red sea rift in afar, *Geology*, *37*(1), 59–62.
Legrand, D., D. Villagómez, H. Yepes, and A. Calahorrano (2004), Multifractal dimension and b-value analysis of the 1998–1999 Quito swarm related to Guagua Pichincha volcano activity, Ecuador, *J. Geophys. Res.*, *109*, B01307, doi:10.1029/2003JB002572.
Maccaferri, F., M. Bonafede, and E. Rivalta (2011), A quantitative study of the mechanisms governing dike propagation, dike arrest and sill formation, *J. Volcanol. Geotherm. Res.*, *208*(1), 39–50, doi:10.1016/j.jvolgeores.2011.09.001.
Maccaferri, F., E. Rivalta, L. Passarelli, and S. Jónsson (2013), The stress shadow induced by the 1975–1984 Krafla rifting episode, *J. Geophys. Res. Solid Earth*, *118*, 1109–1121, doi:10.1002/jgrb.50134.
Maghsoudi, S., S. Hainzl, S. Cesca, T. Dahm, and D. Kaiser (2014), Identification and characterization of growing large-scale en-echelon fractures in a salt mine, *Geophys. J. Int.*, *196*(2), 1092–1105, doi:10.1093/gji/ggt443.
Main, I. G. (1987), A characteristic earthquake model of the seismicity preceding the eruption of Mount St. Helens on 18 May 1980, *Phys. Earth Planet. Inter.*, *49*(3), 283–293.
McNutt, S. (1996), Seismic monitoring and eruption forecasting of volcanoes: A review of the state-of-the-art and case histories, in *Monitoring and Mitigation of Volcano Hazards*, edited by S. McNutt, pp. 99–146, Springer, Berlin.
McNutt, S. R. (2005), Volcanic seismology, *Annu. Rev. Earth Planet. Sci.*, *32*, 461–491, doi:10.1146/annurev.earth.33.092203.122459.
Mogi, K. (1962), Magnitude-frequency relation for elastic shocks accompanying fractures of various materials and some related problems in earthquakes, *Bull. Earthquake Res. Inst.*, *40*, 831–883.
Murru, M., C. Montuori, M. Wyss, and E. Privitera (1999), The locations of magma chambers at Mt. Etna, Italy, mapped by b-values, *Geophys. Res. Lett.*, *26*(16), 2553–2556, doi:10.1029/1999GL900568.
Nakada, S., M. Nagai, T. Kaneko, A. Nozawa, and K. Suzuki-Kamata (2005), Chronology and products of the 2000 eruption of Miyakejima volcano, Japan, *Bull. Volcanol.*, *67*(3), 205–218, doi:10.1007/s00445-004-0404-4.
Okada, Y. (1992), Internal deformation due to shear and tensile faults in a half-space, *Bull. Seismol. Soc. Am.*, *82*(2), 1018–1040.
Ozawa, S., S. Miyazaki, T. Nishimura, M. Murakami, M. Kaidzu, T. Imakiire, and X. Ji (2004), Creep, dike intrusion, and magma chamber deflation model for the 2000 Miyake eruption and the Izu islands earthquakes, *J. Geophys. Res.*, *109*, B02410, doi:10.1029/2003JB002601.
Pallister, J. S., et al. (2010), Broad accommodation of rift-related extension recorded by dyke intrusion in Saudi Arabia, *Nat. Geosci.*, *3*(10), 705–712.
Passarelli, L., F. Maccaferri, E. Rivalta, T. Dahm, and E. A. Boku (2013), A probabilistic approach for the classification of earthquakes as "triggered" or "not triggered", *J. Seismol.*, *17*(1), 165–187.

Richardson, E., and T. H. Jordan (2002), Seismicity in deep gold mines of South Africa: Implications for tectonic earthquakes, *Bull. Seismol. Soc. Am.*, *92*(5), 1766–1782, doi:10.1785/0120000226.
Rivalta, E. (2010), Evidence that coupling to magma chambers controls the volume history and velocity of laterally propagating intrusions, *J. Geophys. Res.*, *115*, B07203, doi:10.1029/2009JB006922.
Rivalta, E., and T. Dahm (2004), Dyke emplacement in fractured media: Application to the 2000 intrusion at Izu Islands, Japan, *Geophys. J. Int.*, *157*, 283–292.
Rivalta, E., B. Taisne, A. Bunger, and R. Katz (2014), A review of mechanical models of dike propagation: Schools of thought, results and future directions, *Tectonophysics*, *638*, 1–42, doi:10.1016/j.tecto.2014.10.003.
Roman, D. C. (2005), Numerical models of volcanotectonic earthquake triggering on non-ideally oriented faults, *Geophys. Res. Lett.*, *32*, L02304, doi:10.1029/2004GL021549.
Rubin, A. M., and D. Gillard (1998), Dike-induced earthquakes: Theoretical considerations, *J. Geophys. Res.*, *103*(B5), 10,017–10,030.
Rubin, A. M., and D. D. Pollard (1988), Dike-induced faulting in rift zones of Iceland and Afar, *Geology*, *16*(5), 413–417, doi:10.1130/0091-7613.
Rubin, A. M., D. Gillard, and J.-L. Got (1998), A reinterpretation of seismicity associated with the January 1983 dike intrusion at Kilauea Volcano, Hawaii, *J. Geophys. Res.*, *103*(B5), 10,003–10,015.
Sanchez, J., S. McNutt, J. Power, and M. Wyss (2004), Spatial variations in the frequency-magnitude distribution of earthquakes at Mount Pinatubo Volcano, *Bull. Seismol. Soc. Am.*, *94*(2), 430–438, doi:10.1785/0120020244.
Scholz, C. (1968), The frequency-magnitude relation of microfracturing in rock and its relation to earthquakes, *Bull. Seismol. Soc. Am.*, *58*(1), 399–415.
Schorlemmer, D., S. Wiemer, and M. Wyss (2005), Variations in earthquake-size distribution across different stress regimes, *Nature*, *437*(7058), 539–542, doi:10.1038/nature04094.
Segall, P. (2013), Volcano deformation and eruption forecasting, *Geol. Soc. London Spec. Publ.*, *380*(1), 85–106, doi:10.1002/2013JB010251.
Shuler, A., and M. Nettles (2012), Earthquake source parameters for the 2010 western Gulf of Aden rifting episode, *Geophys. J. Int.*, *190*(2), 1111–1122.
Stefansson, R., G. Gudmundsson, and P. Halldorsson (2008), Tjörnes Fracture Zone. New and old seismic evidences for the link between the North Iceland rift zone and the Mid-Atlantic ridge, *Tectonophysics*, *447*, 117–126.
Stein, R. S., S. Toda, T. Parsons, and E. Grunewald (2006), A new probabilistic seismic hazard assessment for greater Tokyo, *Philos. Trans. R. Soc. A*, *364*(1845), 1965–1988.
Toda, S., R. S. Stein, and T. Sagiya (2002), Evidence from the AD 2000 Izu islands earthquake swarm that stressing rate governs seismicity, *Nature*, *419*(6902), 58–61, doi:10.1038/nature00997.
Traversa, P., and J.-R. Grasso (2009), Brittle creep damage as the seismic signature of dyke propagations within basaltic volcanoes, *Bull. Seismol. Soc. Am.*, *99*(3), 2035–2043, doi:10.1785/0120080275.
Traversa, P., and J.-R. Grasso (2010), How is volcano seismicity different from tectonic seismicity?, *Bull. Seismol. Soc. Am.*, *100*(4), 1755–1769, doi:10.1785/0120090214.
Traversa, P., V. Pinel, and J. Grasso (2010), A constant influx model for dike propagation: Implications for magma reservoir dynamics, *J. Geophys. Res.*, *115*, B01201, doi:10.1029/2009JB006559.
Uhira, K., T. Baba, H. Mori, H. Katayama, and N. Hamada (2005), Earthquake swarms preceding the 2000 eruption of Miyakejima volcano, Japan, *Bull. Volcanol.*, *67*(3), 219–230, doi:10.1007/s00445-004-0405-3.
Ukawa, M. (1991), Collision and fan-shaped compressional stress pattern in the Izu Block at the northern edge of the Philippine Sea plate, *J. Geophys. Res.*, *96*(B1), 713–728, doi:10.1029/90JB02142.
Ukawa, M., and H. Tsukahara (1996), Earthquake swarms and dike intrusions off the east coast of Izu Peninsula, central Japan, *Tectonophysics*, *253*(3), 285–303.
Utsu, T. (1999), Representation and analysis of the earthquake size distribution: A historical review and some new approaches, *Pure Appl. Geophys.*, *155*(2-4), 509–535.
Warren, N., and G. Latham (1970), An experimental study of thermally induced microfracturing and its relation to volcanic seismicity, *J. Geophys. Res.*, *75*(23), 4455–4464.
Wells, D. L., and K. J. Coppersmith (1994), New empirical relationships among magnitude, rupture length, rupture width, rupture area, and surface displacement, *Bull. Seismol. Soc. Am.*, *84*(4), 974–1002.
White, R. S., J. Drew, H. R. Martens, J. Key, H. Soosalu, and S. S. Jakobsdóttir (2011), Dynamics of dyke intrusion in the mid-crust of Iceland, *Earth Planet. Sci. Lett.*, *304*(3), 300–312, doi:10.1016/j.epsl.2011.02.038.
Wiemer, S., and S. R. McNutt (1997), Variations in the frequency-magnitude distribution with depth in two volcanic areas: Mount St. Helens, Washington, and Mt. Spurr, Alaska, *Geophys. Res. Lett.*, *24*(2), 189–192, doi:10.1029/96GL03779.
Wiemer, S., and M. Wyss (2000), Minimum magnitude of completeness in earthquake catalogs: Examples from Alaska, the Western United States, and Japan, *Bull. Seismol. Soc. Am.*, *90*, 859–869.
Wiemer, S., and M. Wyss (2002), Mapping spatial variability of the frequency-magnitude distribution of earthquakes, *Adv. Geophys.*, *45*, 259–302.
Wiemer, S., S. McNutt, and M. Wyss (1998), Temporal and three-dimensional spatial analyses of the frequency-magnitude distribution near Long Valley Caldera, California, *Geophys. J. Int.*, *134*(2), 409–421.
Woessner, J., and S. Wiemer (2005), Assessing the quality of earthquake catalogues: Estimating the magnitude of completeness and its uncertainty, *Bull. Seismol. Soc. Am.*, *95*(2), 684–698, doi:10.1785/0120040007.
Wright, T., and S. Sakai (2005), Interpretation of the Miyakejima 2000 eruption and dike emplacement using time animations of earthquakes, *Bull. Earthquake Res. Inst.*, *79*(1/2), 1–16.
Wyss, M. (1973), Towards a physical understanding of the earthquake frequency distribution, *Geophys. J. Int.*, *31*(4), 341–359.
Yamaoka, K., M. Kawamura, F. Kimata, N. Fujii, and T. Kudo (2005), Dike intrusion associated with the 2000 eruption of Miyakejima volcano, Japan, *Bull. Volcanol.*, *67*(3), 231–242, doi:10.1007/s00445-004-0406-2.